ROGUE WAVE PATTERNS FOR BOUSSINESQ AND OTHER PHYSICAL EQUATIONS

Adrian Ankiewicz

Department of Fundamental & Theoretical Physics, Research School of Physics
The Australian National University
Canberra ACT 2601, Australia

Received 4 April 2025, accepted 27 June 2025, published online 22 August 2025

We study higher-order rogue wave patterns for the well-known Boussinesq equation for the cases where the solution parameters are large. We show that these consist of a collection of individual fundamental rogue waves arranged in circles. The radii of these circles are found from the zeroes of certain polynomials. Finally, we briefly compare the patterns found with those of higher-order rogue wave patterns of the nonlinear-Schrödinger (NLS) and other equations.

DOI:10.5506/APhysPolB.56.9-A1

1. Principle

The Boussinesq equation was derived by Boussinesq in the 1870s [1, 2], to get a better description of water waves by including a nonlinear part. It applies to weakly nonlinear and reasonably long waves, e.g. in shallow seas and harbours.

Rogue waves supported by this equation are presented in [3], where it was shown that the 'volume' [4] contained by a rogue wave of order n can be conveniently defined. When the solutions are real functions having zero background, there is no need to subtract out any 'background' in order to specify a finite integral over all 2d space.

The Boussinesq equation can be normalized in various ways. In keeping with [3], etc., we use

$$u_{tt} + u_{xx} - (u^2)_{xx} - \frac{1}{3}u_{xxxx} = 0,$$
 (1)

where u is the free surface elevation of the water, t is the time, and x is the transverse direction.

It supports solitons

$$u = \frac{1}{6} (4b^2 - 3) (c^2 - 1) + 2b^2 \operatorname{sech}^2 \left(b \sqrt{\frac{4b^2}{3} - 1} c t - bx \right) ,$$

for $b > \sqrt{3}/2$. When c = 1, this gives the zero-background soliton.

2. Boussinesq equation rogue waves and link with breathers

This equation is significantly different from the NLS in that its solutions are real and also in that it can have rogue waves with zero background, while the NLS cannot support these. Boussinesq equation breathers have been studied in some papers [5–7]. The basic breather can be written as

$$u_b = u_0 + 2\alpha p^2 \frac{f\cos(px) - \alpha}{[f - \alpha\cos(px)]^2},$$
 (2)

where the background is u_0 ,

$$f = \sqrt{r} \cosh \left(\mu + p t \sqrt{\frac{p^2}{3} + 1 - 2u_0} + \frac{1}{2} \log(r) \right),$$

and

$$r = \alpha^2 \frac{4p^2 + 3 - 6u_0}{p^2 + 3 - 6u_0}.$$

Here, α, μ , and frequency p are free parameters, and we need $p^2 + 3 > 6u_0$, ensuring r > 0. An example is shown in Fig. 1.

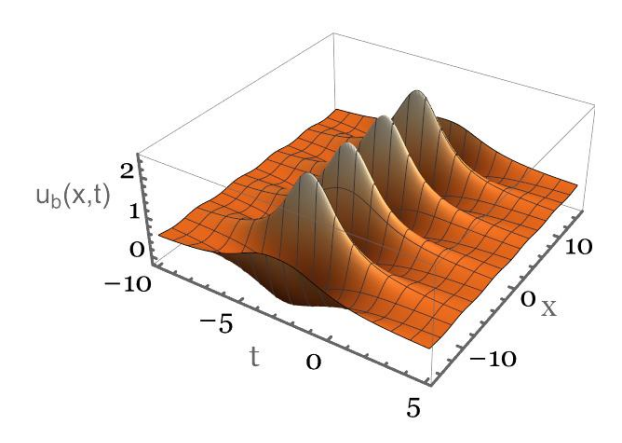


Fig. 1. Boussinesq equation n=1 breather. Here, $p=\mu=\alpha=1; u_0=1/2.$

Now, setting $\mu = -\frac{1}{2}\log(r)$ allows the maximum to occur at t=0. As p decreases, the peaks move further apart, and, in the limit of small p, we have the rogue wave

$$u_b = u_0 - 4 \frac{(2u_0 - 1) \left[t^2 (1 - 2u_0)^2 - (1 - 2u_0)x^2 + 1 \right]}{\left[t^2 (1 - 2u_0)^2 + (1 - 2u_0)x^2 + 1 \right]^2},$$
 (3)

assuming that $u_0 < \frac{1}{2}$, so the solution is finite everywhere. Also, u_0 can be negative. Here, the background level, u_0 , also scales the dimensions of the rogue wave. The maximum value is $u_b(0,0) = 4 - 7u_0$. As u_0 increases to 1/2, this maximum value falls to 1/2. An example is shown in Fig. 2.

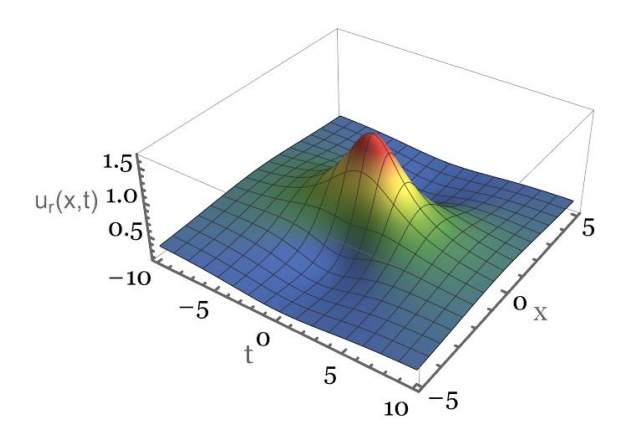


Fig. 2. Boussinesq equation n=1 rogue wave. Here, background $u_0=1/3$. The maximum value is $u_b(0,0) = 5/3$.

Indeed,

$$u(x,t) = d_1 + 2\frac{\partial^2}{\partial x^2} \log \left[\hat{F}_1(t,x)\right],$$

where $d_1 = \frac{u_0}{2(1-2u_0)}\hat{F}_1$ and $\hat{F}_1 = t^2(1-2u_0)^2 + (1-2u_0)x^2 + 1$. Further, if $u_0 = 0$, then $d_r = 0$, $f\cos(px) - \alpha \approx \frac{\alpha}{2}p^2(t^2 - x^2 + 1)$, and $f - \alpha \cos(px) \approx \frac{\alpha}{2}p^2(t^2 + x^2 + 1)$, so from Eq. (3), we have

$$u_b = u_1 = \frac{4(t^2 - x^2 + 1)}{(t^2 + x^2 + 1)^2} = 2\frac{\partial^2}{\partial x^2} \log \left[\hat{F}_1(t, x)\right],$$

where $\hat{F}_1 = 1 + x^2 + t^2$, and this coincides with the regular zero-background first-order rogue wave [3]. We note the NLS rogue wave cannot have zero background [13], while such rogue waves do exist for the Boussinesq equation.

In fact, the n^{th} -order solution can be written as

$$u_n = 2\frac{\partial^2}{\partial x^2} \log \left[\hat{F}_n(t, x) \right] = \frac{2}{\hat{F}_n^2} \left[\hat{F}_n \hat{F}_n'' - \left(\hat{F}_n' \right)^2 \right], \tag{4}$$

where \hat{F}_n can include solution parameters. Thus, the entire solution [8] depends on the single function F_n . However, for the NLS, the intensity depends on a single function but the entire solution cannot be found from it. This occurs because the NLS solutions are complex and have phase information, while the Boussinesq solutions are real and do not have phase. Clearly, the component rogue waves will appear when the function F_n has a small value, and so this is the function to be considered.

We note that each solution with zero background has a quantized value for its 'volume' [3] defined as

$$V_n = \frac{1}{8\pi} \int_{-\infty}^{\infty} \int_{-\infty}^{\infty} u_n^2 \, dt \, dx = \frac{1}{2} n(n+1) = Q_n.$$
 (5)

Here, $Q_n = (1, 3, 6, 10, ...)$ is the n^{th} triangle number. Furthermore,

$$W_n = \frac{1}{8\pi} \int_{-\infty}^{\infty} \int_{-\infty}^{\infty} u_n^3 dt dx = n(n+1) = 2Q_n.$$
 (6)

We can define a related integrand, using

$$v_n = -2\frac{\partial^2}{\partial x \,\partial t} \,\log \left[\hat{F}_n(t,x)\right] \,. \tag{7}$$

Then

$$E_n = \frac{1}{8\pi} \int_{-\infty}^{\infty} \int_{-\infty}^{\infty} v_n^2 dt dx = \frac{1}{6} n(n+1) = \frac{1}{3} Q_n.$$
 (8)

These are proved in [3]. For example, for the fundamental (n = 1) rogue wave, derived from $\hat{F}_1 = 1 + x^2 + t^2$, we have $V_1 = 1$, $W_1 = 2$, and $E_1 = 1/3$.

For the nonzero background $u_0(<1/2)$, we need to subtract off the background before integrating. We find

$$V_1 = \frac{1}{8\pi} \int_{-\infty}^{\infty} \int_{-\infty}^{\infty} (u_1 - u_0)^2 dt dx = \sqrt{1 - 2u_0}.$$
 (9)

Also,

$$W_1 = \frac{1}{8\pi} \int_{-\infty}^{\infty} \int_{-\infty}^{\infty} (u_1 - u_0)^3 dt dx = 2(1 - 2u_0)^{3/2}.$$
 (10)

Knowing the volume (or W_1) from experimental measurements can allow us to determine the background level, u_0 .

These quantizations of the volumes apply for any values of the parameters included in the solutions [8], and show the special nature of the Boussinesq rogue waves. By measuring the total volume of a rogue wave structure in an experiment that is governed by the Boussinesq equation, one could infer the order, n, of the formation.

For high values of the free parameters, the approximations become asymptotically exact.

2.1. Second-order
$$(n=2)$$
 Boussinesq

Taking the free (real) parameters to be (a, b), we now write the form of the second-order (n = 2) Boussinesq rogue wave from [3]:

$$\hat{F}_2 = F_2 + 2atP_1 + 2bxQ_1 + (a^2 + b^2) F_0, \qquad (11)$$

with $F_0 = 1$.

Then

$$F_2 = (t^2 + x^2)^3 + \frac{1}{9} \left[51t^4 + 5t^2 \left(54x^2 + 95 \right) + 25 \left(3x^4 - 5x^2 + 25 \right) \right] ,$$

while

$$P_1 = 3x^2 - t^2 + \frac{5}{3},$$

$$Q_1 = x^2 - 3t^2 - \frac{1}{3},$$

and $F_0 = 1$. It is easy to verify that $V_2 = 3$, $W_2 = 6$, and $E_2 = 1$. We plot an example of the exact result in Figs. 3 and 4. The overall maximum of 5.5 occurs for a = 0, b = 7.5 at t = 0, x = -1.8. This is an asymmetric case. If a = b = 0, the solution is clearly symmetric in (x, t); the maximum of 4.85 occurs at t = 0, $x = \pm 1.33$.

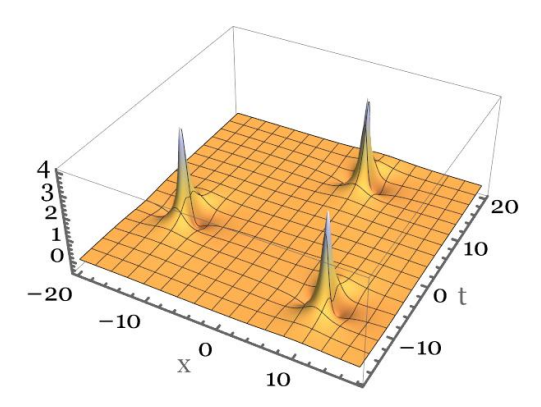


Fig. 3. Exact second-order (n = 2) case, using equations (4) and (11). Here, a = 2000 and b = 2000.

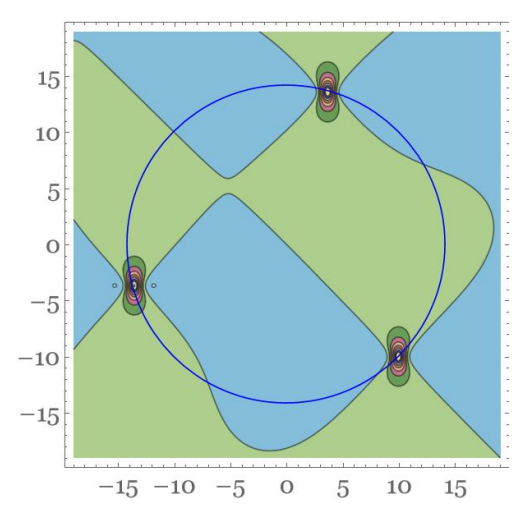


Fig. 4. Exact contours (x,t) for the second-order (n=2) case. Here, a=b=2000. Thus, the (un-normalized) radius of the circle should be $(a^2+b^2)^{1/6}\approx 14.1421$. This plot shows that this is correct.

Here, retaining only high-order terms (of order 6, noting that a, b are of order 3), the required form is

$$\hat{F}_2 \approx a^2 - 2at(t^2 - 3x^2) + b^2 + 2bx(x^2 - 3t^2) + (t^2 + x^2)^3$$
.

Taking $z = -\frac{i(a-ib)^{1/3}}{2^{2/3}}Z$, $x = (z+z^*)/2$, $t = (z-z^*)/(2i)$, and retaining terms of order 6 only (noting a, b are each of order 3), we find

$$\frac{1}{16} \left(Z^3 + 4 \right) \, \left[\left(Z^* \right)^3 + 4 \right] \left(a^2 + b^2 \right) = 0 \, .$$

Hence, $JJ^*=0$, so $J=Z^3+c_2^2=0$, with $c_2=2$ and the formation consists of 3 individual basic rogue waves on a circle of radius $|Z|=|Z_1|=2^{2/3}\approx 1.5874$, as above. This is a Yablonskii–Vorob'ev polynomial, viz. $Q_2^{(1)}=Z^3+4$. Such polynomials are related to the Painlevé equations [8–10]. Its zeros are plotted in Fig. 5. In un-normalized co-ordinates, we have the radius as $r=|z|=2^{-2/3}|a-ib|^{1/3}|Z_1|=(a^2+b^2)^{1/6}$.

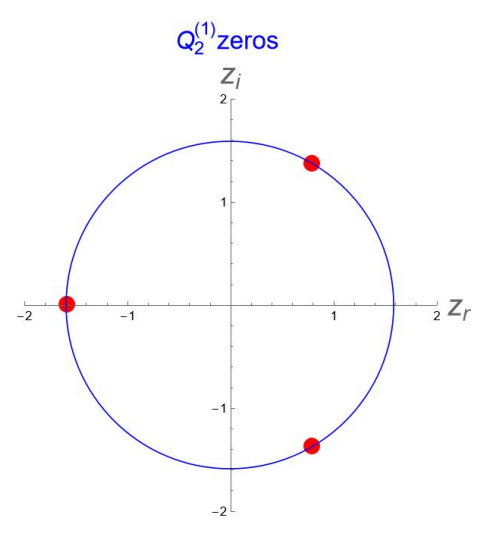


Fig. 5. Second-order (n=2) case. Zeros of $Q_2^{(1)} = Z^3 + 4$, shown as red dots, with $Z = Z_r + i Z_i$. The circle radius is $|Z_1| = 2^{2/3} \approx 1.5874$. The individual rogue wave positions match those in the exact plots, as seen in Figs. 3 and 4.

2.2. Third-order (n=3) Boussinesq triangle formation

Here, we take a = b = 0. We obtain the exact results using the procedure from [11] (not repeated here). It is easy to verify that $V_3 = 6$, $W_3 = 12$, and $E_3 = 2$. We plot an example in Figs. 6 (3d format) and 7 (contour format).

Now, we retain only the high-order terms (of order 12), noting that the parameters are of order 3. Then, for high values of the parameters (g, h), the function \hat{F}_3 is proportional to

$$\begin{aligned} &-25g^4 + 50g^3 t \left(t^2 - 3x^2\right) - 5g^2 \left[10h^2 - 10hx \left(x^2 - 3t^2\right)\right. \\ &+ 3t^6 + 45t^4x^2 - 15t^2x^4 + 7x^6\right] - 10gt \left(t^2 - 3x^2\right) \\ &\times \left[-5h^2 - 4hx \left(x^2 - 3t^2\right) + \left(t^2 + x^2\right)^3\right] \\ &- 25h^4 + 50h^3x \left(x^2 - 3t^2\right) - 5h^2 \left(7t^6 - 15t^4x^2 + 45t^2x^4 + 3x^6\right) \\ &- 10hx \left(x^2 - 3t^2\right) \left(t^2 + x^2\right)^3 - \left(t^2 + x^2\right)^6 \; .\end{aligned}$$

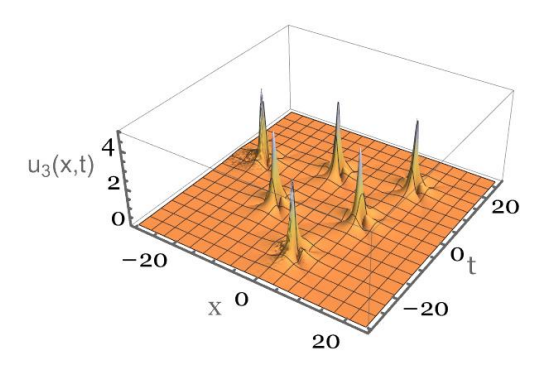


Fig. 6. Third-order (n=3) 'triangle' case. This is plotted using the exact results. Here, g=h=1000, while the other 2 solution parameters are zero. The positions of the individual rogue wave components match those of the YVP polynomial zeroes, as seen in Fig. 8.

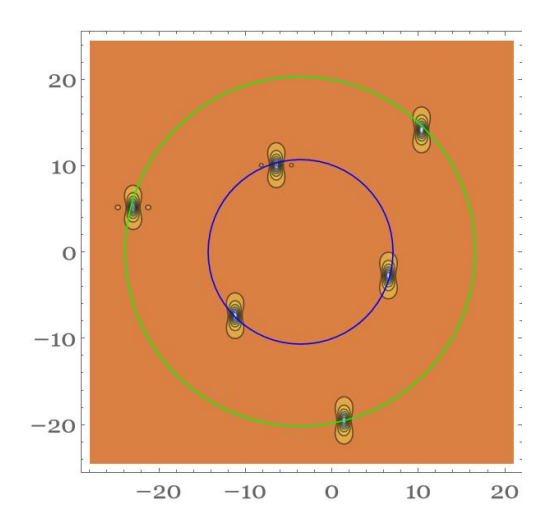


Fig. 7. Exact contours (x,t) for the third-order (n=3) 'triangle' case. Here, g=h=1000, while the other 2 parameters are zero. Thus, the (un-normalized) radius of the inner circle should be $|Z_1|(g^2+h^2)^{1/6}/2^{2/3}\approx 10.65$, while that of the outer circle should be $|Z_2|(g^2+h^2)^{1/6}/2^{2/3}\approx 20.23$. This plot shows that these are correct.

Now, setting

$$z = \frac{iZ(g+ih)^{1/3}}{2^{2/3}},$$
(12)

and $x = (z + z^*)/2$, $t = (z - z^*)/(2i)$, we get

$$\frac{1}{256} \left(Z^6 + 20Z^3 - 80 \right) \left[\left(Z^* \right)^6 + 20 \left(Z^* \right)^3 - 80 \right] \left(g^2 + h^2 \right)^2 = 0,$$

so that $PP^* = 0$, where $P = Z^6 + 20Z^3 - 80$ and this is the polynomial $Q_3^{(1)}$.

The 6 zeros of this polynomial occur on 2 circles. Normalized radii $|Z_1|$ and $|Z_2|$ are given in the caption of Fig. 8. Thus, the (un-normalized) radii are found, from equation (12), as $|z| = |Z|(g^2 + h^2)^{1/6}/2^{2/3}$.

Then, the radius of the inner circle should be $|Z_1|(g^2+h^2)^{1/6}/2^{2/3} \approx 10.65$, while that of the outer circle should be $|Z_2|(g^2+h^2)^{1/6}/2^{2/3} \approx 20.23$. These agree with the values seen in Fig. 6.

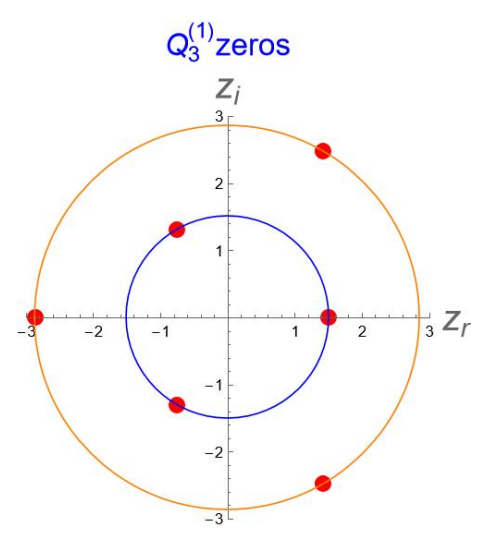


Fig. 8. Third-order (n=3) case. Zeros of $Q_3^{(1)}=Z^6+20Z^3-80$, are shown as red dots, with $Z=Z_r+i\,Z_i$. The positions of the individual rogue wave components match those of the exact results, as seen in Figs. 6 and 7. The circles have radii $|Z_1|=[2(3\sqrt{5}-5)]^{1/3}\approx 1.50611$ and $|Z_2|=[2(3\sqrt{5}+5)]^{1/3}\approx 2.86093$. The individual rogue wave positions match those in the exact plots, as seen in Figs. 6 and 7.

2.3. Third-order (n=3) Boussinesq ring formation

Here, we take g = h = 0 and plot the exact results in Figs. 9 and 10, using [3]. It is easy to verify that $V_3 = 6$, $W_3 = 12$, and $E_3 = 2$. Thus,

$$\hat{F}_3 = F_3 + 2atP_2 + 2bxQ_2 + (a^2 + b^2) F_1.$$

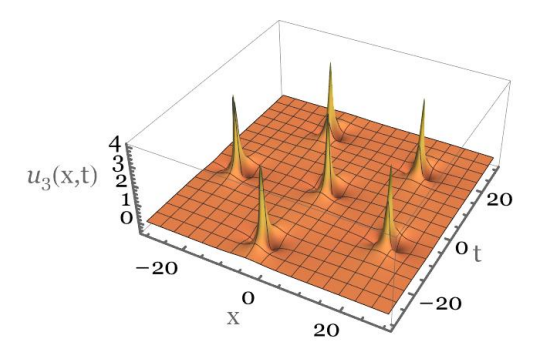


Fig. 9. Third-order (n=3) 'ring' case (exact). Here, $a=b=5\times 10^6$ and the other 2 parameters are zero.

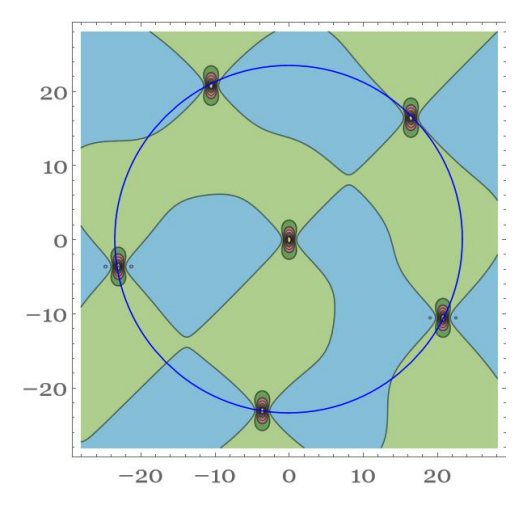


Fig. 10. Exact contours for third order (n=3) 'ring' case. Here $a=b=5\times 10^6$ and the other 2 parameters are zero. Here, the circle radius is 23.437.

Now, retaining only high-order terms (of order 12, noting that a, b are each of order 5)

$$F_3 \approx \left(t^2 + x^2\right)^6 \,,$$

while

$$P_2 \approx (t^2 + x^2) (t^4 - 10t^2x^2 + 5x^4) ,$$

 $Q_2 \approx (t^2 + x^2) (5t^4 - 10t^2x^2 + x^4) ,$

and

$$F_1 \approx t^2 + x^2$$
.

Then

$$\hat{F}_3 \approx (t^2 + x^2) \left[a^2 + 2a t \left(t^4 - 10t^2 x^2 + 5x^4 \right) + b^2 + 2b x \left(5t^4 - 10t^2 x^2 + x^4 \right) + \left(t^2 + x^2 \right)^5 \right].$$

Taking $z = -\frac{iZ(a-ib)^{1/5}}{2^{4/5}3^{2/5}}$, and $x = (z+z^*)/2$, $t = (z-z^*)/(2i)$, and retaining terms of order 6 only, as above, we get

$$|Z|^2(Z^5 - 144) \left[(Z^*)^5 - 144 \right] = 0.$$

Hence $KK^* = 0$, with $K = Z(Z^5 - c_3^2) = 0$, where $c_3 = 12$, and the formation consists of 5 individual basic rogue waves on a circle of radius $|Z_3| = 2^{4/5}3^{2/5} \approx 2.70192$, and one as a nucleus in the centre. This is the YVP [12]

$$Q_3^{(2)} = Z \left(Z^5 - 144 \right) . (13)$$

Its zeros are plotted in Fig. 11. In un-normalized co-ordinates, we have the radius as $r = |z| = \frac{|a-ib|^{1/5}|Z|}{2^{4/5}3^{2/5}} = |Z_3| \frac{(a^2+b^2)^{1/10}}{2^{4/5}3^{2/5}} = (a^2+b^2)^{1/10}$. For the plotted case, $a = b = 5 \times 10^6$, this radius is 23.437. (See Figs. 9 and 10.)

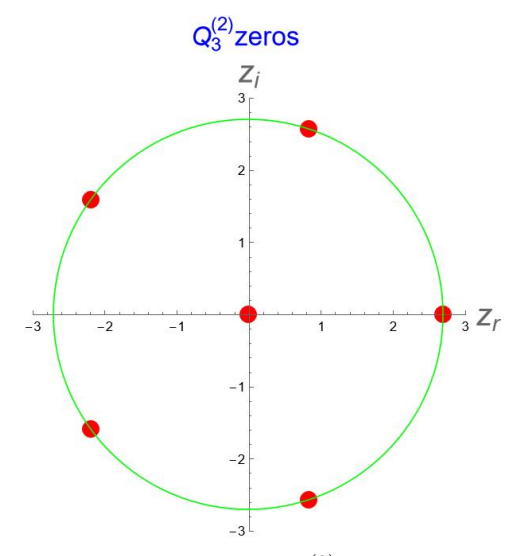


Fig. 11. Third-order (n=3) case. Zeros of $Q_3^{(2)} = Z(Z^5 - 144)$. The (normalized) radius is $2^{4/5}3^{2/5} \approx 2.7$. The individual rogue wave positions match those in the exact plots, as seen in Figs. 9 and 10.

2.4. Fourth-order
$$(n = 4)$$
 Boussinesq

The fourth order (n = 4) Boussinesq rogue wave is found from [3]. Now

$$\hat{F}_4 = F_4 + 2atP_3 + 2bxQ_3 + (a^2 + b^2) F_2.$$

Here, retaining only high-order terms (of order 20, noting that a, b are each of order 7)

$$F_4 \approx \left(t^2 + x^2\right)^{10} \,,$$

while

$$P_3 \approx -(t^2 + x^2)^3 (t^6 - 21t^4x^2 + 35t^2x^4 - 7x^6),$$

 $Q_3 \approx -(t^2 + x^2)^3 (7t^6 - 35t^4x^2 + 21t^2x^4 - x^6),$

and

$$F_2 \approx \left(t^2 + x^2\right)^3.$$

Then

$$\hat{F}_4 \approx (t^2 + x^2)^3 \left[a^2 - 2at \left(t^6 - 21t^4x^2 + 35t^2x^4 - 7x^6 \right) + b^2 + 2bx \left(-7t^6 + 35t^4x^2 - 21t^2x^4 + x^6 \right) + \left(t^2 + x^2 \right)^7 \right].$$

Taking
$$z = -\frac{iZ(a-ib)^{1/7}}{2^{6/7}15^{2/7}}$$
, $x = (z+z^*)/2$, $t = (z-z^*)/(2i)$, and writing out

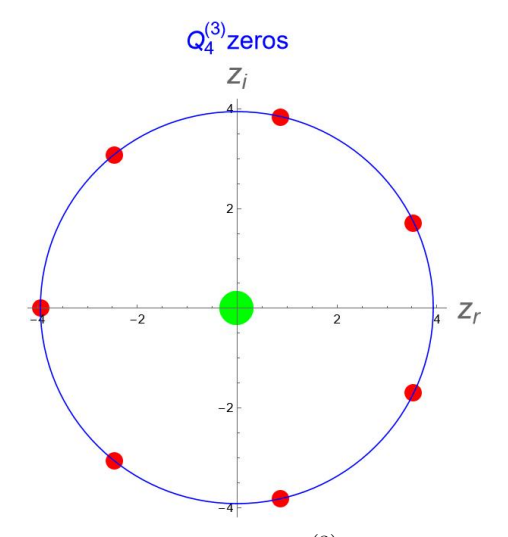


Fig. 12. Fourth-order (n=4) case. Zeros of $Q_4^{(3)}=Z^3(Z^7+14400)$. The (normalized) radius is $2^{6/7}15^{2/7}\approx 3.926$.

 \hat{F}_4 , we find that $KK^* = 0$, with $K = Z^3(Z^7 + c_4^2) = 0$, where $c_4 = 120$, and the formation consists of 7 individual basic rogue waves on a circle of radius $|Z| = 2^{6/7}15^{2/7} \approx 3.92692$, and 3 as a (large) nucleus in the centre, as seen in Fig. 12. This is the YVP $Z^3(Z^7 + 14400) = Q_4^{(3)}$ [8]. In un-normalized co-ordinates, we have the radius as $r = |z| = \frac{|a-ib|^{1/7}|Z|}{2^{6/7}15^{2/7}} = \frac{(a^2+b^2)^{1/14}|Z|}{2^{6/7}15^{2/7}}$.

2.5. Fifth- and higher-order Boussinesa roques

The fifth-order (n=5) Boussinesq rogue wave is found from [3]. Now

$$\hat{F}_5 = F_5 + 2atP_4 + 2bxQ_4 + (a^2 + b^2) F_3.$$

Here, retaining only high-order terms (of order 30, noting that a, b are each of order 9)

$$F_5 \approx (t^2 + x^2)^{15}$$
,

while

$$P_4 \approx (t^2 + x^2)^6 (t^8 - 36t^6x^2 + 126t^4x^4 - 84t^2x^6 + 9x^8) ,$$

$$Q_4 \approx (t^2 + x^2)^6 (9t^8 - 84t^6x^2 + 126t^4x^4 - 36t^2x^6 + x^8) ,$$

and, as above,

$$F_3 \approx \left(t^2 + x^2\right)^6 .$$

Then

$$\hat{F}_5 \approx (t^2 + x^2)^6 \left[a^2 + 2a \left(t^9 - 36t^7 x^2 + 126t^5 x^4 - 84t^3 x^6 + 9tx^8 \right) \right. \\ \left. + b^2 + 2b \left(9t^8 x - 84t^6 x^3 + 126t^4 x^5 - 36t^2 x^7 + x^9 \right) + \left(t^2 + x^2 \right)^9 \right].$$

We note that $P_4 + Q_4 \approx 2(t^2 + x^2)^4 P_2 Q_2$. Taking $z = -\frac{iZ(a-ib)^{1/9}}{2^{8/9}105^{2/9}}$, $x = (z+z^*)/2$, $t = (z-z^*)/(2i)$, and writing out \hat{F}_5 , we find that $KK^* = 0$, with $K = Z^6(Z^9 - c_5^2) = 0$, where $c_5 = 1680$ and the formation consists of 9 individual basic rogue waves on a circle of radius $|Z| = 2^{8/9} 105^{2/9} \approx 5.20877$, and 6 as a (large) nucleus in the centre. This is the YVP $Z^6(Z^9 - 2822400) = Q_5^{(4)}$ [8]. It is plotted in Fig. 13. It is the same equation as in the corresponding NLS case, even though the equations are quite different. In un-normalized co-ordinates, we have the radius as $r = |z| = \frac{|a-ib|^{1/9}|Z|}{2^{8/9}105^{2/9}} = (a^2 + b^2)^{1/18}$. The n = 6 and n = 7 cases are given in Figs. 14 and 15.

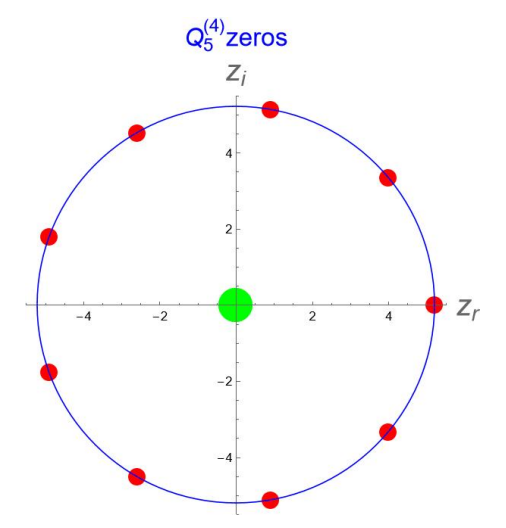


Fig. 13. Fifth-order (n=5) case. Zeros of $Q_5^{(4)}=Z^6(Z^9-c_5^2)$, where $c_5=1680$. The circle radius is $|Z|=2^{8/9}105^{2/9}\approx 5.20877$.

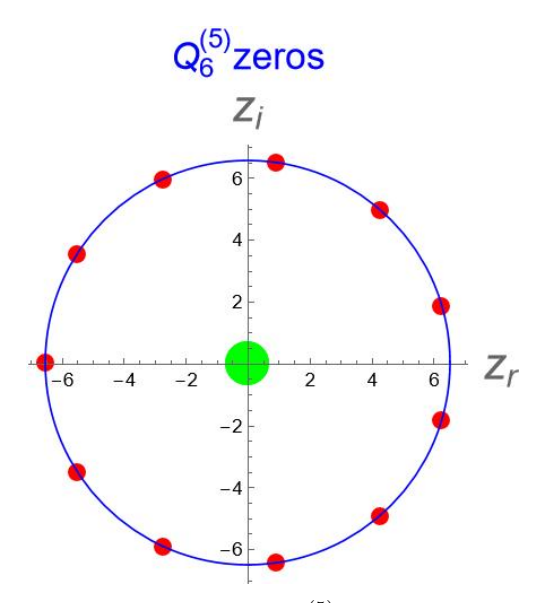


Fig. 14. Sixth-order (n=6) case. Zeros of $Q_6^{(5)}=Z^{10}(Z^{11}+c_6^2)$, where $c_6=30240$. The circle radius is $|Z|=2^{10/11}3^{6/11}35^{2/11}\approx 6.526$.

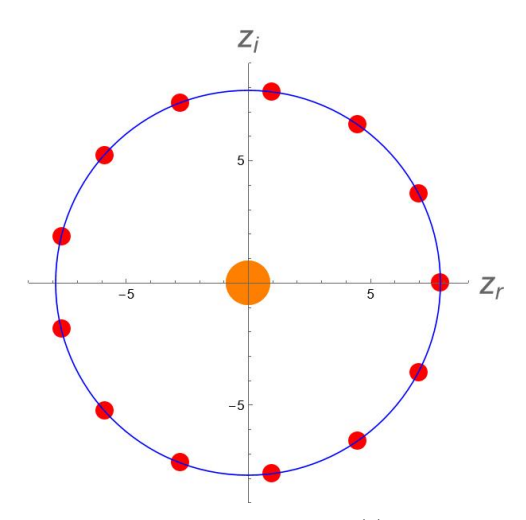


Fig. 15. Seventh-order (n=7) case. Zeros of $Q_7^{(6)} = Z^{15}(Z^{13} - c_7^2)$, where $c_7 = 665280$.

2.6. Boussinesq rogue waves summary

We are considering high-order ring-type rogue waves where the parameters are large, e.g. $a^2 + b^2 \gg 1$. Then $F_n \approx (t^2 + x^2)^{\frac{n}{2}(n+1)}$.

For a given n, with $n \geq 2$, the integer appearing in the YVP $Q_n^{(n-1)}$ is $(-1)^n c_n^2$, where

$$c_n = \frac{[2(n-1)]!}{(n-1)!} = \frac{\Gamma(2n-1)}{\Gamma(n)},$$

where Γ is the Gamma function. Thus, $c_{n+1} = 2(2n-1)c_n$ and $c_n = 2(2n-3)c_{n-1}$. Here, the c_n coefficients are called 'quadruple factorial numbers'.

In fact, the YVP relevant for the n^{th} -order single-ring rogue wave is

$$Q_n^{(n-1)} = Z^{\frac{1}{2}(n-1)(n-2)} \left[Z^{2n-1} + (-1)^n c_n^2 \right] .$$

Hence, the normalized radius is

$$R = |Z| = c_n^{\frac{2}{2n-1}} \approx 1.238n - 0.963$$

in this range of n.

Thus, there are $\frac{1}{2}(n-1)(n-2)$ quanta in the nucleus and 2n-1 quanta in the ring, making a total of $\frac{n}{2}(n+1)$ quanta. These are the triangle numbers [4].

Orders are summarized in Table 1, while coefficients and radii are given in Table 2.

Table 1. Order of solution parameters O(a,b), order of polynomials $P,Q: O(P_n,Q_n)$, order of polynomial (F_n) , integer coefficient c_n that relates to the number $(-1)^n c_n^2$ appearing in the YVP $Q_n^{(n-1)}$.

\overline{n}	O(a,b)	$O(P_n, Q_n, F_n, \hat{F}_n)$	c_n	$(-1)^n c_n^2$
2	3	6	2	4
3	5	12	12	-144
4	7	20	120	14400
5	9	30	1680	-2822400
6	11	42	30240	914457600
\overline{n}	2n-1	n(n+1)	$\frac{[2(n-1)]!}{(n-1)!}$	

Table 2. Values of n, c_n , and then c_n/c_{n-1} , normalized radius for the single ring, as a fraction and then as a decimal number. In fact, in this range, the normalized radius is roughly 1.238n - 0.963.

n	c_n	c_n/c_{n-1}	Radius	Radius
2	2	2	$2^{2/3}$	1.5874
3	12	6	$2^{4/5}3^{2/5}$	2.70192
4	120	10	$2^{6/7}15^{2/7}$	3.92692
5	1680	14	$2^{8/9}105^{2/9}$	5.20877
6	30240	18	$2^{10/11}3^{6/11}35^{2/11}$	6.52606
\overline{n}	$\frac{[2(n-1)]!}{(n-1)!}$	2(2n-3)		

3. Comparison with high-order rogue waves of the NLS equation

3.1. NLS principle

The NLS,

$$iu_x + \frac{1}{2}u_{tt} + |u|^2 u = 0, (14)$$

is significantly different as its solutions are complex, while those of the Boussinesq equation are real. The NLS describes the envelope (not the wave height directly) of weakly nonlinear deep water waves.

Furthermore, the Boussinesq equation rogue waves can have zero background, while NLS equation rogue waves always have nonzero background [3, 13].

We look at the NLS solutions to make a brief comparison with the main (Boussinesq) part of this paper. We show up similarities and differences.

A rogue wave of n^{th} order of the NLS can be written as [13]

$$\psi_n(x,t) = \left[\frac{G_n(x,t) + iH_n(x,t)}{D_n(x,t)} + (-1)^n \right] e^{ix}.$$
 (15)

In fact, the intensity relative to the background depends only on the denominator term

$$|\psi_n(x,t)|^2 - 1 = [\log(D_n)]_{tt}$$
.

We note that such a relation only gives the intensity, while for the Boussinesq equation, the similar relation, equation (4), gives the full solution. The volume of the NLS rogue wave can be defined [4], but u_n^2 in equation (5) is replaced by $(|\psi_n|^2 - 1)^2$. However, the NLS does not have integer relations corresponding to equations (6) and (8) (i.e. W_n and E_n) of the Boussinesq equation.

Now, (x,t) are real and D_n is never zero, so the solutions are finite everywhere. The intensity is only high when D_n is near to zero, and we can find these positions by studying D_n and only keeping high-order terms, with z = x + it.

Indeed, these positions generally turn out to occur on circles and the radius is then given by $r = |z| = \sqrt{x^2 + t^2}$. Some solutions can be viewed as triangular formations [14], but it can be more convenient to view all as consisting of circles.

3.2. Second order
$$(n=2)$$

For ψ_2 , the denominator D_2 , with free parameters β, γ , is given in [15]. In D_2 , we then just retain large terms (order 6), *i.e.* those of order z^6 , noting that terms β, γ are taken as $3^{\rm rd}$ order. This then reduces to

$$\hat{D}_2 = \beta^2 - 16\beta t \left(t^2 - 3x^2 \right) + \gamma^2 - 16\gamma x \left(x^2 - 3t^2 \right) + 64 \left(t^2 + x^2 \right)^3.$$

We call this function \hat{D}_2 because it approximates D_2 for large β, γ . Let $x=(z+z^*)/2, \ t=\frac{(z-z^*)}{2i}$, so that z=x+it, as noted above. Of course, z increases with β, γ . To normalize, we let $z=-\frac{iZ(\beta+i\gamma)^{1/3}}{2\ 2^{2/3}}$. Then

$$D_2 \approx \frac{1}{16} (\beta^2 + \gamma^2) (Z^3 + 4) [(Z^*)^3 + 4].$$

The positions of the individual rogue waves correspond to zeros of the function $P = Z^3 + 4$. In fact, this is the YVP $Q_2^{(1)}$, matching the function found in Section 2.1. The 3 basic rogue waves thus appear at the positions of the zeros on a circle of radius $|Z| = 2^{2/3}$, as plotted in Fig. 5.

With the normalized form, the radius of the circle is always $|Z| = 2^{2/3} \approx 1.5874$, *i.e.* it is independent of the free parameters. In un-normalized coordinates, we have the radius as $r = |z| = 2^{-5/3} |\beta + i\gamma|^{1/3} |Z| = \frac{1}{2} (\beta^2 + \gamma^2)^{1/6}$, agreeing with [15].

3.3. Third order
$$(n=3)$$
 — Nucleus with 1 ring

In D_3 , we just retain large terms, *i.e.* those of order z^{12} (with $\beta = 0$, $\gamma = 0$ and taking parameters a_{5r} and a_{5i} to be 5th order). We call this function \hat{D}_3 because it approximates D_3 for large a_{5r} and a_{5i} . Then

$$\hat{D}_{3} = 4096 (t^{2} + x^{2}) \left[2025 a_{5i}^{2} + 90 a_{5i} (5t^{4}x - 10t^{2}x^{3} + x^{5}) + 2025 a_{5r}^{2} + 90 a_{5r} (t^{5} - 10t^{3}x^{2} + 5tx^{4}) + (t^{2} + x^{2})^{5} \right].$$

Then with $x = (z + z^*)/2$ and $t = \frac{z-z^*}{2i}$: to normalize, we define

$$z = -\frac{i5^{1/5}}{2^{4/5}} Z (a_{5r} - ia_{5i})^{1/5} ,$$

and then D_3 factors to

$$\hat{D}_3 = 100 \ 10^{2/5} \left(a_{5i}^2 + a_{5r}^2 \right)^{6/5} |Z|^2 \left(Z^5 - 144 \right) \left[(Z^*)^5 - 144 \right] .$$

This can be written as $JJ^* = 0$, where

$$J = Z(Z^5 - 144)$$
.

This is the same polynomial as in equation (13) in Section 2.3.

Thus, $D_3 = 0$ means that J = 0, where $J = Z(Z^5 - 144)$. This is $Q_3^{(2)} = Z(Z^5 - 144)$, and its zeros are plotted in Fig. 11. It is the same equation as in the corresponding Boussinesq case, even though the equations are quite different. Thus, one basic rogue wave will appear at the origin (Z = 0), while another 5 will be equi-spaced on a circle of radius $2^{4/5}3^{2/5} \approx 2.70192$. In fact, an example is given in [4]. This one resembles the Boussinesq ring formation studied above in Section 2.3.

In un-normalized co-ordinates, we have the radius as $r=|z|=\frac{5^{1/5}}{2^{4/5}}(a_{5r}^2+a_{5i}^2)^{1/10}|Z|=45^{1/5}(a_{5r}^2+a_{5i}^2)^{1/10}$.

3.4. Third-order
$$(n=3)$$
 2 rings case

Here, we keep only high (12th) order terms (taking β and γ to be 3rd order and $a_{5r} = 0$, $a_{5i} = 0$). We call this function \bar{D}_3 because it approximates D_3 for large β and γ . We get

$$\bar{D}_{3} = 25\beta^{4} + 400\beta^{3} (t^{3} - 3tx^{2}) + 10\beta^{2} [5\gamma^{2} - 40\gamma (3t^{2}x - x^{3}) +32 (3t^{6} + 45t^{4}x^{2} - 15t^{2}x^{4} + 7x^{6})] -80\beta t (t^{2} - 3x^{2}) [-5\gamma^{2} + 32\gamma x (x^{2} - 3t^{2}) + 64 (t^{2} + x^{2})^{3}] +25\gamma^{4} - 400\gamma^{3} (3t^{2}x - x^{3}) + 320\gamma^{2} (7t^{6} - 15t^{4}x^{2} + 45t^{2}x^{4} + 3x^{6}) -5120\gamma x (x^{2} - 3t^{2}) (t^{2} + x^{2})^{3} + 4096 (t^{2} + x^{2})^{6}.$$

Let $x = (z + z^*)/2$, $t = \frac{z-z^*}{2i}$, and set

$$z = -\frac{i}{2^{5/3}}(\beta + i\gamma)^{1/3}Z$$
.

Thus,

$$\bar{D}_3 = \frac{\left(\beta^2 + \gamma^2\right)^2}{256} \left(Z^6 + 20Z^3 - 80\right) \left[(Z^*)^6 + 20 (Z^*)^3 - 80 \right].$$

Setting this to zero implies that $KK^* = 0$ with $K = Z^6 + 20Z^3 - 80$. Hence

$$Z^6 + 20Z^3 - 80 = 0$$

is needed for the positions of the individual rogue waves. This is $Q_3^{(1)}$, and its zeros are plotted in Fig. 8. It is the same function as in the corresponding Boussinesq case, Section 2.2, even though the equations are quite different. There are 2 circles, of radii $|Z_1| = [2(3\sqrt{5}-5)]^{1/3} \approx 1.50611$ and $|Z_2| = [2(3\sqrt{5}+5)]^{1/3} \approx 2.86093$, each with 3 zeros on them. Thus, there are 6 individual fundamental rogue waves.

In un-normalized co-ordinates, we have the radii as $r_{1,2}=|z_{1,2}|\approx 2^{-5/3}|\beta+i\gamma|^{1/3}|Z_{1,2}|=2^{-5/3}(\beta^2+\gamma^2)^{1/6}|Z_{1,2}|$. Then

$$r_{1,2} \approx 2^{-5/3} \left(\beta^2 + \gamma^2\right)^{1/6} \left[2\left(3\sqrt{5} \pm 5\right)\right]^{1/3}$$

so that $r_1 \approx 0.474395 (\beta^2 + \gamma^2)^{1/6}$, while $r_2 \approx 0.901135 (\beta^2 + \gamma^2)^{1/6}$.

4. Relation to other physical equations

More general equations have been considered in [16–19], such as

$$iu_x + \frac{1}{2}u_{tt} + |u|^2 u + i\gamma \left(|u|^2 u\right)_t + i(\mu - 2\gamma)u \left(|u|^2\right)_t + \frac{1}{2}(\mu - \gamma)(\mu - 2\gamma)|u|^4 u = 0.$$
(16)

If $\gamma = 0$, it reduces to the Kundu–Eckhaus equation. If μ is also zero, it gives the NLS, Eq. (14). The Chen–Lee–Liu equation arises when $\gamma = \mu$. The Kaup–Newell (KN) equation is the $\gamma = \mu/2$ case. Further, $\mu = 0$ gives the Gerdjikov–Ivanov equation that has applications in photonic crystal fibres and nonlinear fibre optics. Characteristics of rogue waves of these equations have been presented in [17]. Similar patterns for some large-parameter rogue waves for such integrable systems are shown in [18].

Taking the KN equation in the form given in [20], retaining only the large terms in the denominator, we have

$$D/16 = 96 \left\{ mt \left[\left(1 - 12\beta^2 \right) t^2 - 12\beta tx - 3x^2 \right] + n(2\beta t + x) \left[\left(4\beta^2 - 3 \right) t^2 + 4\beta tx + x^2 \right] \right\} + 256 \left[\left(4\beta^2 + 1 \right) t^2 + 4\beta tx + x^2 \right]^3 + 9 \left(m^2 + n^2 \right) ,$$

where we have transformed $x \to 2x$ to preserve circles in the reduction $(\beta = 0)$ to the NLS form. As β increases up to 0.4, say, the 3 component first-order rogue waves are still approximately on circles, but their centres are no longer the origin. The radius is still proportional to $(m^2 + n^2)^{1/6}$.

5. Conclusion

We have derived higher-order rogue wave patterns for the Boussinesq equation, where the solution parameters are large and shown that these consist of at least one ring of individual fundamental rogue waves, where the radii of these circles are determined from the zeroes of Yablonskii–Vorob'ev polynomials.

We have briefly compared these results with other equations occurring in physics, pointing out similarities and differences.

REFERENCES

- [1] J. Boussinesq, «Théorie de l'intumescence liquide, appelée onde solitaire ou de translation se propagente dans un canal rectangulaire», *Comptes Rendus* **72**, 755 (1871).
- [2] J. Boussinesq, «Théorie des ondes et des remous qui se propagent le long d'un canal rectangulaire horizontal, en communiquant au liquide contenu dans ce canal des vitesses sensiblemant parielles de la surface au fond», J. Math. Pures Appl. 17, 55 (1872).
- [3] A. Ankiewicz, A.P. Bassom, P.A. Clarkson, E. Dowie, «Conservation Laws and Integral Relations for the Boussinesq Equation», Stud. Appl. Math. 139, 104 (2017).
- [4] A. Ankiewicz, N. Akhmediev, «Multi-rogue waves and triangular numbers», Rom. Rep. Phys. 69, 104 (2017). See Fig. 3.
- [5] Y. Liu, B. Li, A.-M. Wazwaz, «Novel high-order breathers and rogue waves in the Boussinesq equation via determinants», *Math. Meth. Appl. Sci.* **43**, 3701 (2020).
- [6] X. Li, X. Yin, N. Cao, L. Xu, «Rogue-wave solutions of a Boussinesq equation from Rossby waves with the generalized β -effect in a barotropic fluid of atmospheric science», *Chinese J. Phys.* **96**, 1232 (2025).
- [7] Y.-L. Ma, «N-solitons, breathers and rogue waves for a generalized Boussinesq equation», *Int. J. Comput. Math.* **97**, 1648 (2020).
- [8] P.A. Clarkson, «Remarks on the Yablonskii-Vorob'ev polynomials», *Phys. Lett. A* 319, 137 (2003).
- [9] F. Balogh, M. Bertola, T. Bothner, «Hankel determinant approach to generalized Vorob'ev-Yablonski polynomials and their roots», *Constr. Approx.* 44, 417 (2016).
- [10] M. Musette, «Painlevé Analysis for Nonlinear Partial Differential Equations», in: R. Conte (Ed.) «The Painlevé Property One Century Later», Springer-Verlag, Berlin 1998, pp. 517–572, see equations (2.140)–(2.143), arXiv:solv-int/9804003.
- [11] B. Yang, J. Yang, «General Rogue Waves in the Boussinesq Equation», J. Phys. Soc. Jpn. 89, 024003 (2020).
- [12] P.A. Clarkson, E.L. Mansfield, «The second Painlevé equation, its hierarchy and associated special polynomials», *Nonlinearity* **16**, R1 (2003),
- [13] N. Akhmediev, A. Ankiewicz, J.M. Soto-Crespo, «Rogue waves and rational solutions of the nonlinear Schrödinger equation», *Phys. Rev. E* 80, 026601 (2009). See Table 1.
- [14] D.J. Kedziora, A. Ankiewicz, N. Akhmediev, «Triangular rogue wave cascades», *Phys. Rev. E* **86**, 056602 (2012).
- [15] A. Ankiewicz, D.J. Kedziora, N. Akhmediev, «Rogue wave triplets», *Phys. Lett. A* 375, 2782 (2011).

- [16] S. Chen et al., «Super chirped rogue waves in optical fibers», Opt. Express 27, 11370 (2010).
- [17] A. Ankiewicz, A. Chowdury, «Analysis of characteristics of rogue waves for higher-order equation», Nonlinear Dyn. 109, 1069 (2022).
- [18] B. Yang, J. Yang, «Universal rogue patterns associated with the Yablonskii–Vorob'ev polynomial hierarchy», *Physica D* 425, 132958 (2021), see Eq. (3).
- [19] A. Ankiewicz, «Rogue and semi-rogue waves defined by volume», Nonlinear Dyn. 104, 4241 (2021).
- [20] X. Wang *et al.*, «Higher-order rogue wave solutions of the Kundu–Eckhaus equation», *Phys. Scr.* **89**, 095210 (2014).